Materials Science in Semiconductor Processing 115 (2020) 105102

Contents lists available at ScienceDirect

Materials Science in Semiconductor Processing

journal homepage: http://www.elsevier.com/locate/mssp

Full length article

Few-layer $PdSe_2$-based field-effect transistor for photodetector applications

A. Venkatesan [a], Servin Rathi [a], Yunseob Kim [a], Hanul Kim [b], Dongmok Whang [b,c], Sun Jin Yun [d], Gil-Ho Kim [a,b,*]

[a] School of Electronic and Electrical Engineering, Sungkyunkwan University, Suwon, 16419, Republic of Korea
[b] Samsung-SKKU Graphene Centre, Sungkyunkwan Advanced Institute of Nanotechnology (SAINT), Sungkyunkwan University, Suwon, 16419, Republic of Korea
[c] School of Advanced Materials Science and Engineering, Sungkyunkwan University, Suwon, 16419, Republic of Korea
[d] ICT Components and Materials Technology Research Division, Electronics and Telecommunications Research Institute, Daejeon, 34129, Republic of Korea

ARTICLE INFO

Keywords:
Photodetector
Palladium diselenide
Two-dimensional materials
Photoresponse
Field effect transistor

ABSTRACT

We demonstrate a multilayer palladium diselenide ($PdSe_2$) high-performance photodetector. The photodetector exhibits the photodetectivity of 0.15×10^{10} Jones under laser illumination ($\lambda = 655$ nm and power of 0.057 $mWmm^{-2}$). The negative threshold voltage shift in transfer characteristics upon laser illumination is mainly attributed to the photogating effect. Systematic analysis of experimental data indicates that the photogating effect and space charge limited conduction are simultaneously involved in the conduction mechanism. We observe that the photogenerated current increases logarithmically as the light intensity increases, and it persists (~200 s) even after stopping the illumination. The slow decrease in current was attributed to the trapping of photogenerated charge carriers at the $PdSe_2/SiO_2$ interface and the defects in the structure of $PdSe_2$. We also observe a reproducible and stable time-resolved photoresponse with respect to the incident laser power. We believe that this study can be an important source of information and can help researchers to continue to investigate methods that would allow them to maximise the potential of $PdSe_2$ for photodetector applications.

1. Introduction

Owing to their excellent electrical and optical properties, two-dimensional (2D) materials have attracted the interest of researchers for photodetection applications [1–4]. These materials are considered to be potential candidates for replacing conventional silicon-based materials in state-of-the-art ultrafast photodetectors [5–7]. Recent publications have reported the remarkable characteristics of such 2D materials, including their broad waveband detection from ultraviolet to THz frequencies, ultrahigh photoresponsivity, polarization-sensitive photodetection, and high-speed photoresponse [8–10].

Among various 2D layered materials, transition metal chalcogenides (TMDs), where one layer of transition metal atoms is sandwiched between two layers of chalcogen atoms, have been considered for the improvement of the existing functionalities of photodetectors or achieving new ones, such as physical flexibility, high detectivity, efficiency or wavelength range, and transparency [11–14]. Owing to their atomic thickness, TMDs interact strongly with light; this results in their excellent optoelectronic properties which can be modulated using local fields, such as gate-voltage-induced electric, ferroelectric, and magnetic fields [15–17]. Gate-voltage-induced electric fields also facilitate the tuning of the transport properties and carrier density in atomic-thin channels, which can decrease the dark current to relatively low levels and create great potential for infrared photodetection [18].

Palladium diselenide ($PdSe_2$) is the noble TMD with 2D pentagonal structure. It possesses puckered lattice structure with Pd atoms in the middle covalently bonded to four Se atoms, two of which are located respectively in the top and in the bottom part. The two neighbouring Se atoms located in the top and bottom sublayers form tilted Se–Se dumbbell (with puckering distance of ≈1.6 Å) crossing the Pd layer, resulting in a lack of rotational symmetry [19]. This structure is potentially sensitive to defects, as Se vacancy (V_{Se}) would break the symmetry of the Se-Se dumbbell and induce large structural distortion. This is in contrast with the commonly observed layered hexagonal TMDs, where the symmetry remains intact even at a relatively high concentration of chalcogen vacancy. Further, in comparison to other TMDs, the puckered 2D $PdSe_2$ flakes exhibit widely tunable band gap that varies from ~1.3 eV for monolayer to 100 meV or less depending on their thickness. Such high bandgap tunability is one of the most remarkable properties of $PdSe_2$ in comparison to other 2D

* Corresponding author. School of Electronic and Electrical Engineering, Sungkyunkwan University, Suwon, 16419, Republic of Korea.
E-mail address: ghkim@skku.edu (G.-H. Kim).

https://doi.org/10.1016/j.mssp.2020.105102
Received 30 December 2019; Received in revised form 4 March 2020; Accepted 26 March 2020
Available online 4 April 2020

semiconducting material [20,21].

In addition, few-layer $PdSe_2$ based field-effect transistors (FETs) have displayed tunable ambipolar charge carrier conduction with a high electron field-effect mobility of ~158 $cm^2V^{-1}s^{-1}$ [22]. These extraordinary electronic properties of $PdSe_2$ hold great potential for future optoelectronic, piezoelectric, spintronic, and valleytronic applications.

In this study, we fabricated n-type $PdSe_2$ FET using quasi-one-dimensional nanobelt shaped $PdSe_2$ flakes from a commercially available source and the conventional exfoliation technique. We studied the optoelectronic properties of the $PdSe_2$ FET at Room temperature (RT) at the wavelength of 655 nm and it was found that it exhibited excellent photodetectivity. We also analysed the stability and reproducibility of the as-prepared 2D $PdSe_2$ FET by performing time-resolved photoresponse measurements. We believe that this study could help researchers to address key concerns and challenges, such as charge traps and photogating that are associated with $PdSe_2$ for photodetection applications.

2. Experimental detail

For the fabrication of the $PdSe_2$ FET, $PdSe_2$ flakes were obtained from commercially available bulk $PdSe_2$ (2D Semiconductors, USA). Subsequently, a few $PdSe_2$ layers were transferred onto a heavily doped p-type silicon substrate with thermally grown SiO_2 (285 nm thick), using the conventional exfoliation technique. Suitable flakes were identified using an optical microscope and their thickness was confirmed using atomic force microscopy (AFM). Optical and e-beam lithography techniques were used for outer and inner metal electrode patterning. The deposition of Cr (10 nm) and Au (100 nm) was carried out using an e-beam evaporator at the pressure of 1×10^{-6} Torr. After the evaporation of the metal, the sample was soaked in acetone for 45 min to lift-off the excess metal followed by cleaning with isopropyl alcohol and nitrogen blowing.

3. Results and discussion

Raman spectroscopy and AFM were used to analyse the optical properties and thickness of the $PdSe_2$ flakes. The Raman spectrum of the few-layer flake was obtained at RT using a 532 nm laser (Fig. 1(a)) and confirmed that the few-layer flake was $PdSe_2$. The three peaks observed at 143, 205, and 225 cm^{-1} (denoted as A_g^1, A_g^2, and B_{1g}, respectively) could be assigned to the movement of Se atoms, and the highest peak observed at 258 cm^{-1} was ascribed to the relative movement of the Pd and Se atoms [19,20]. It is interesting to note that all of four peaks involve vibrations of Se atoms. This can be attributed to unique crystal structure of $PdSe_2$ in which each layer is actually a Se-Pd-Se trilayer with Pd atoms covalently bonded to four Se atoms on the top and bottom sublayers. The more detailed information on the relative movement of each atom corresponding to the observed Raman peak can be found elsewhere [19,22]. We also observed that the Raman peaks of $PdSe_2$ were slightly upshifted with respect to theoretical peaks of bulk $PdSe_2$ and were consistent with the estimated number of layers. This upshift in the Raman peaks can be attributed to interlayer coupling and hybridization resulting from the size reduction. Fig. 1(b) illustrates the AFM image of $PdSe_2$, where the thickness of the $PdSe_2$ layers was measured along the red line with indicator and was determined to be 11.2 nm (~18 layers).

Electrical measurements of the $PdSe_2$ FET were carried out using a 4200 SCS parameter analyser (Keithley, USA) under ambient conditions and in the dark. Before electrical measurements, the as-prepared devices were spin coated with poly (methyl methacrylate) (PMMA) for 30 s at 5000 rpm followed by vacuum annealing at 300 °C for 2 h. The pressure

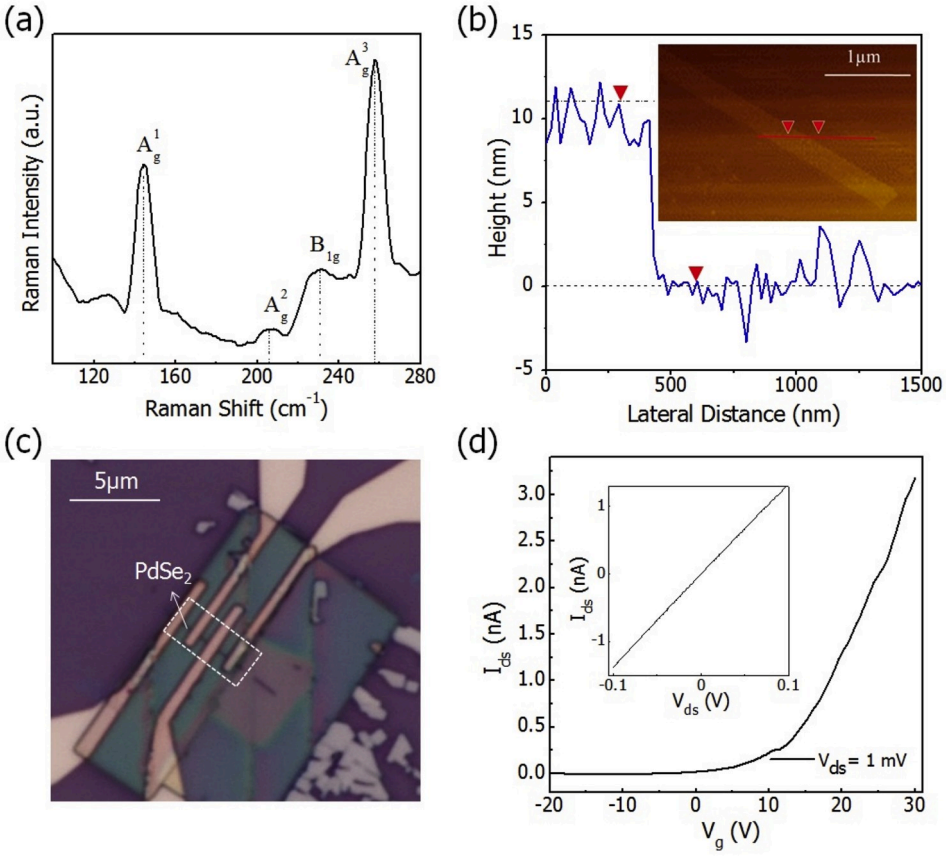

Fig. 1. (a) Raman spectrum of $PdSe_2$. (b) AFM image (inset) and line profile of $PdSe_2$ along the red line with thickness indicator. (c) Optical microscopy image of $PdSe_2$ FET. (d) Transfer characteristics of $PdSe_2$ FET (inset: I_{ds} *vs.* V_{ds} of $PdSe_2$ in the dark) under ambient conditions.

of the vacuum chamber during annealing was maintained at 1×10^{-6} Torr. The photodetector characteristics of the $PdSe_2$ FET were measured under the illumination of laser light ($\lambda = 655$ nm) of various incident powers. Fig. 1(c) depicts the optical microscopy image of the as-prepared $PdSe_2$ phototransistor. The length (L) and width (W) of the nanobelt were determined to be 0.81 and 0.47 μm, respectively. Fig. 1 (d) and its inset illustrate the I_{ds} *vs.* V_{ds} and transfer characteristics (I_{ds} *vs.* V_g) of the $PdSe_2$ FET at room temperature. The linear relationship between the I_{ds} and V_{ds} indicates good electrical contacts between Cr/Au and $PdSe_2$.

The multilayer $PdSe_2$ presented n-type conduction behaviour, with field-effect mobility (μ_{FE}) of 3.9 $cm^2V^{-1}s^{-1}$. The observed low mobility of our sample can be attributed to trapped water and oxygen molecules during various steps in sample fabrication as well as other factors like interface contacts, layer thickness etc [23–25]. The on/off current ratio was determined to be 10^4. The μ_{FE} was calculated using the equation $\mu_{FE} = (L/W) \times (g_m/C_{ox}V_{ds})$, where g_m is the transconductance, and C_{ox} is the dielectric capacitance between the channel and back-gate per unit area. In this study, we used the slope of the I_{ds} *vs.* V_g curve to obtain g_m, and C_{ox} was calculated using the equation: $C_{ox} = \varepsilon_0\varepsilon_r/d$, where ε_r is the relative permittivity of SiO_2, ε_0 is the permittivity of free space, and d is the thickness of SiO_2 [26,27]. The threshold voltage (V_t) was determined to be ~14 V. To investigate the optoelectronic properties of the device, we carried out transport measurements under the illumination of laser ($\lambda =$ 655 nm) under ambient conditions. The photocurrent (I_{ds}^{Photo}) under laser illumination was calculated using the following equation [28]:

$$I_{ds}^{Photo} = I_{ds}^{Light} - I_{ds}^{Dark}, \quad (1)$$

where I_{ds}^{Light} and I_{ds}^{Dark} are the drain-source currents under laser illumination and in the dark, respectively.

Fig. 2(a) depicts the transfer characteristics of the $PdSe_2$ FET with and without laser light illumination (the illumination power of the laser was 0.057 $mWmm^{-2}$). The linearity of the device was maintained intact under laser illumination and further analysis indicates that laser illumination has negligible effect on μ_{FE}. However, laser illumination significantly changed the threshold voltage ($V_t \sim 5$ V) by shifting the transfer characteristic in the negative direction ($\Delta V_t \sim -9$V). The off current significantly increases by more than one order of magnitude upon illumination (blue line in Fig. 2(a)). The impression of ambipolar behaviour in Fig. 2 (a) is actually due to the saturation current in the off region and is usually attributed to several factors including gate leakage, interface charge trap induced current or band to band tunneling due to lowering of barrier in the negative gate regime for hole transport. Thus, it can be safely concluded that the observed pA current in the negative gate voltage regime is due to gate leakage current.

From Fig. 2 (b), it can be inferred that I_{ds}^{Photo} strongly depended on V_g. The I_{ds}^{Photo} increases as V_g becomes increasingly positive. This could be attributed to the trapping of the photogenerated holes and electrons at the interface trap sites. In general, under illumination, two different effects are known to occur in field effect phototransistors depending upon the applied V_g, namely the photogating and photoconductive effects (PG and PC, respectively) [29]. Hence, the photocurrent is the sum of two contributions:

$$I_{ds}^{Photo} = I_{ds}^{PG} + I_{ds}^{PC}. \quad (2)$$

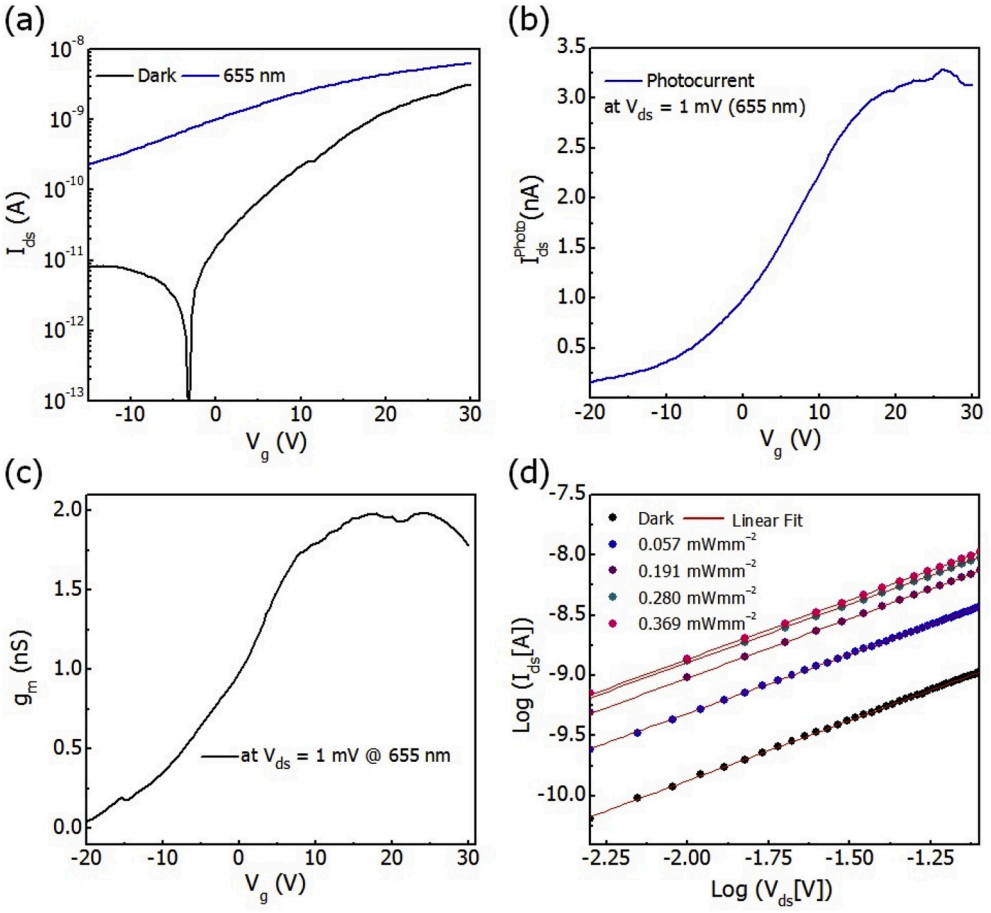

Fig. 2. (a) Transfer characteristics of $PdSe_2$ FET in the dark and under laser illumination ($\lambda = 655$ nm) under ambient conditions. (b) Photocurrent of $PdSe_2$-based photodetector (I_{ds}^{Photo}) as function of gate voltage (V_g). (c) Transconductance (g_m) of $PdSe_2$ photodetector as function of V_g. (d) Log–plot of I_{ds} *vs.* V_{ds} of $PdSe_2$ FET measured at different illumination powers (red line indicates the linear fit).

Generally, the PG effect manifest itself as the change in the transistor threshold voltage, from V_t in the dark to $V_t + \Delta V_t$ under illumination. This enhance the photocurrent, which can be expressed as follows:

$$I_{ds}^{PG} = g_m \cdot |\Delta V_t| = \frac{AKT}{q} \ln\left(1 + \frac{\eta q P_{in}}{I_{pd} h\nu}\right) \quad (3)$$

$$I_{ds}^{PC} = \frac{W}{L} V_{ds} \Delta\sigma \quad (4)$$

where $g_m = \frac{dI_{ds}}{dV_g}$ is the transconductance of the transistor, A is a fitting parameter, K is the Boltzmann constant, T is the absolute temperature, q is the unit of charge, η the quantum efficiency, P_{in} is the incident optical power, I_{pd} is the dark current for holes, and $h\nu$ is the photon energy [29–32]. According to equation (3), the dependence of I_{ds}^{PG} on V_g is the same as that of g_m and it scales logarithmically with P_{in}. Similarly, according to equation (4), the PC effect refers to the increase in conductivity, $\Delta\sigma$, owing to the photogeneration of electron–hole pairs in the channel and is less dependent on V_g. The strong similarity between the dependences of I_{ds}^{Photo} and g_m on V_g can be observed by comparing the graphs in Fig. 2(b) and (c). Therefore, we concluded that the photoresponse from the $PdSe_2$ FET was mainly due to the PG effect, because I_{ds}^{PC} was not expected to depend on V_g significantly. Typically, the PG effect originates from the traps that are located in the channel or at the channel/gate insulator interface, where they act as additional back gates that become charged upon optical excitation and result in photogating the device and consequently shift the threshold voltage.

To better understand the conduction mechanism in the channel, we plotted I_{ds} *vs.* V_{ds} for various laser powers in log scale (Fig. 2(d)). The current follows the simple power law: $I_{ds} \propto V_{ds}^{\gamma}$, where $\gamma \leq 1$. The calculated values of γ decreased from 1.001 ± 0.002 to 0.951 ± 0.009 as P_{in} increased from 0 (in the dark) to 0.369 $mWmm^{-2}$. That is γ decreased gradually as P_{in} was increased from 0 (dark) to 0.369 $mWmm^{-2}$. The calculated γ values were less than 1 at all illumination powers. Therefore, the conduction mechanism attributed to the Child–Langmuir (CL) law (where $I \propto V^{3/2}$), where the current is space charge–limited (SCL), could be omitted [33]. For a solid that contains numerous traps, the SCL conduction mechanism can be typically described using the Mark–Helfrich law: $I \propto V^{l+1}$, where $l = T_c/T > 1$ and T_c is a parameter that characterises the exponential distribution of the energy of the traps [31,34]. Based on the traditional SCL models for solids, $\gamma \geq 2$. This indicates that the traditional SCL models for solids could not be used to explain the γ values (lower than 2) obtained in our experiments. This inconsistency between the model and our experimental data could be resolved by considering an SCL model for band gap materials, where $\gamma = 3/2$, which is similar to the CL law at the limit of the ultra-relativistic regime [29,31,35]. The γ values that are lower than 3/2 should be attributed to other quantum phenomena like quantum CL law where the scaling is $1/2 \leq \gamma \leq 3/2$ [36]. At higher illumination power, the SCL conduction is transformed into an ohmic one owing to the higher number of photogenerated carriers and the improved screening of localised trapped charges. The dependence of I_{ds} on P_{in} at higher voltages is weaker than at lower voltages (Fig. 2(d)). This may be attributed to the SCL mechanism becoming more dominant at lower drain bias than at higher voltage.

Fig. 3(a) presents the schematic illustration of the $PdSe_2$-based photodetector under laser irradiation and Fig. 3(b) illustrates the I_{ds} *vs.* V_{ds} characteristics of the $PdSe_2$-based photodetector in the dark and under laser irradiation ($\lambda = 655$ nm) at various effective P_{in} values. As P_{in} increased, I_{ds} also increased (Fig. 3(b)).

To better understand the characteristics of the photodetector, we calculated the photoresponsivity (R) of the $PdSe_2$-based phototransistor at $V_g = 0$ V from the photoresponse curve (Fig. 4(a)), as a function of P_{in} at $\lambda = 655$ nm and $V_{ds} = 1$ mV using the following equation [37]:

$$R = \frac{I_{Photo}}{P_{in}} = \frac{(I_{laser} - I_{dark})}{P_{in}}, \quad (5)$$

where I_{laser} is the current of the device under laser light irradiation and I_{dark} is the current measured in the dark. As P_{in} was decreased from 0.369 to 0.057 $mWmm^{-2}$, R increased from 88.5 to 161.9 AW^{-1} (Fig. 4(b)).

Afterward, we calculated the specific detectivity of the device; this is another performance index of photodetectors, which is relevant to the sensitivity of detectors. Fig. 4(c) illustrates the dependences of R and $D^*$of the $PdSe_2$-based photodetectors on P_{in} at $\lambda = 655$ nm and $V_{ds} = 1$ mV. Assuming that the shot noise from I_{dark} is the major contributor to the total noise, D^* could be calculated as follows:

$$D^* = \frac{RS^{1/2}}{(2qI_{dark})^{1/2}}, \quad (6)$$

where S is the active area of the photodetector [38,39]. The maximum R and D^* values of the $PdSe_2$-based photodetector under laser irradiation ($\lambda = 655$ nm) were calculated to be 161.9 AW^{-1} and 1.51×10^9 Jones, respectively. These values are comparable with those previously reported in the literature [40,41]. During the photosensing measurements, V_{ds} was constantly biased at 1 mV which is significantly lower than the values used in previous studies. These excellent R and D^* values could be attributed to the nanobelt like structure of $PdSe_2$.

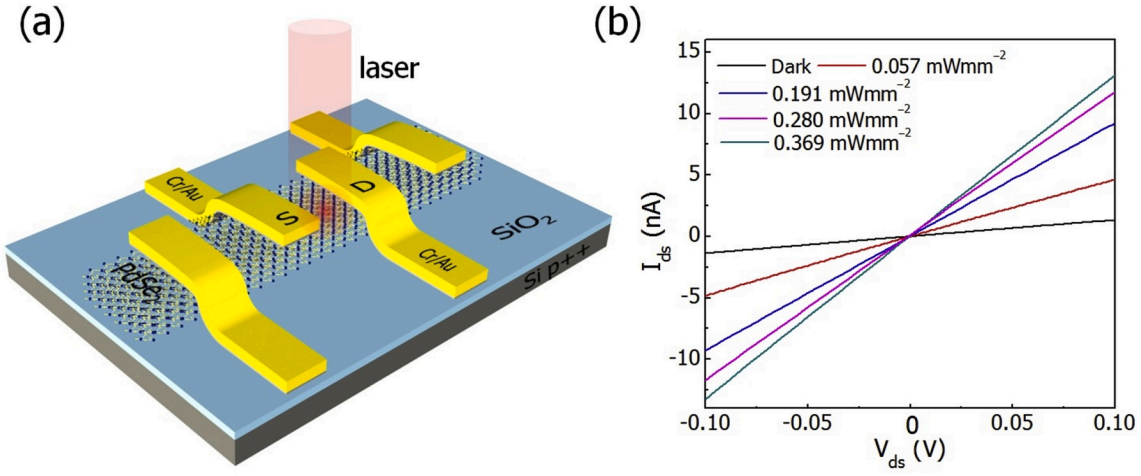

Fig. 3. (a) Schematic representation of few-layer $PdSe_2$-based photodetector under laser illumination. During the photodetection measurements, the $PdSe_2$ photodetector was protected with cross-linked PMMA. (b) I_{ds} *vs.* V_{ds} of $PdSe_2$-based photodetector measured at different incident optical powers under ambient conditions.

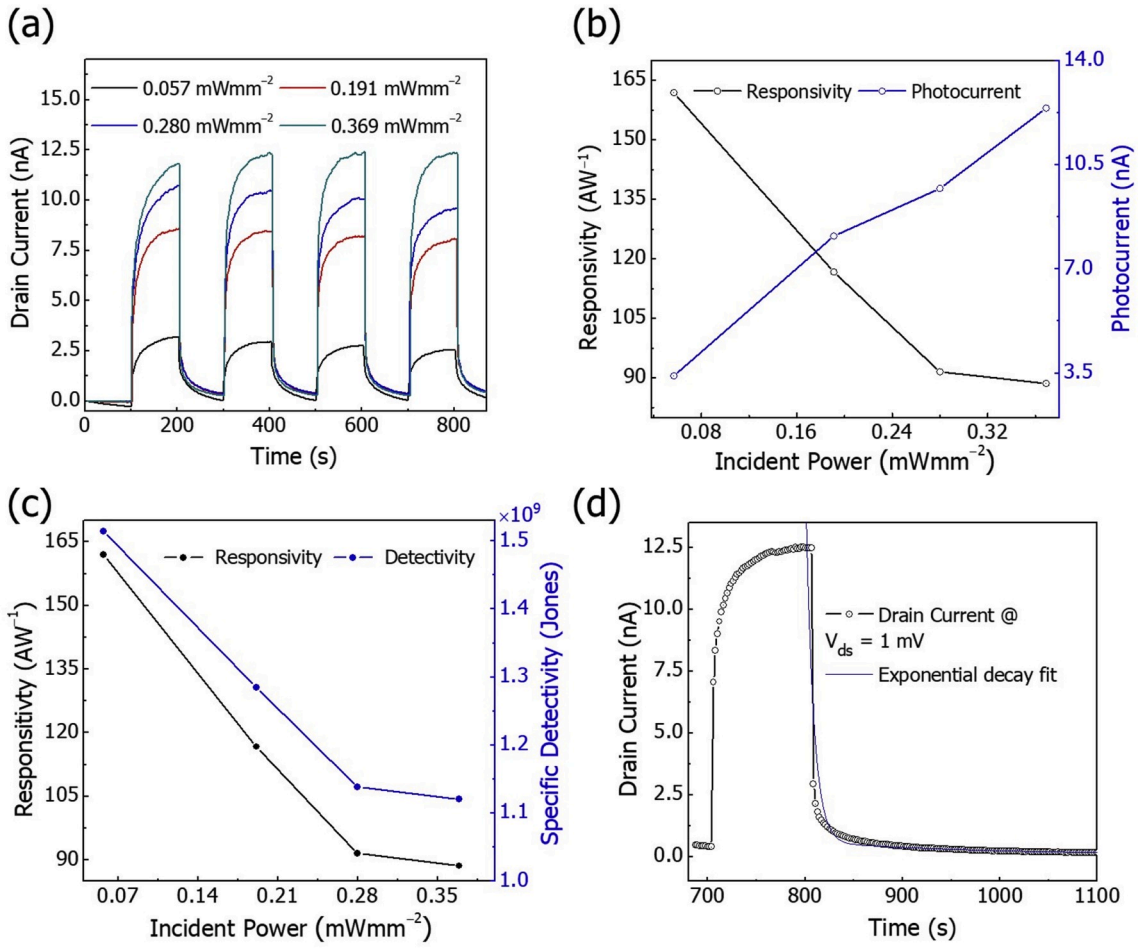

Fig. 4. (a) Time-resolved photoresponse of $PdSe_2$-based photodetector at different illumination incident power (P_{in}) values at λ = 655 nm measured at ambient conditions. (b) Photoresponsivity (R) and photocurrent of $PdSe_2$-based photodetector at different P_{in} values measured under ambient conditions. (c) R and Detectivity (D^*) of $PdSe_2$-based photodetector under ambient conditions. (d) Decrease in drain-source photocurrent (I_{ds}) of $PdSe_2$-based photodetector measured at P_{in} = 0.369 mWmm^{-2} under ambient conditions (the blue line represents the exponential decay fit of I_{ds}).

Using the time-resolved photoresponse of the device at various P_{in} values at λ = 655 nm and V_{ds} = 1 mV, we concluded that the photodetector exhibits repeatable and stable response to the incident laser beam. From Fig. 4(a), we could further infer that the photoresponse of the detector is reproducible at all P_{in} values, which confirm the stability of the $PdSe_2$-based photodetector. In addition, we analysed the transient characteristics of the phototransistor by measuring the channel current (Fig. 4(d)). As soon as the light was turned on, an abrupt increase in I_{ds} was observed followed by a much slower increase. This behaviour could be explained by considering that the trapping of the photogenerated holes that attracts more electrons, which gradually increase the conductivity of the channel (Fig. 5(a) and (b)). But when the light was switched off I_{ds} slowly decreased. This occurred because the trapped charges (PG effect) prolonged the conductivity despite the absence of illumination. The decay curve could be fitted using two exponentials with shorter ($t_1 \sim 8$ s) and longer ($t_2 \sim 200$ s) time constants [31,42]:

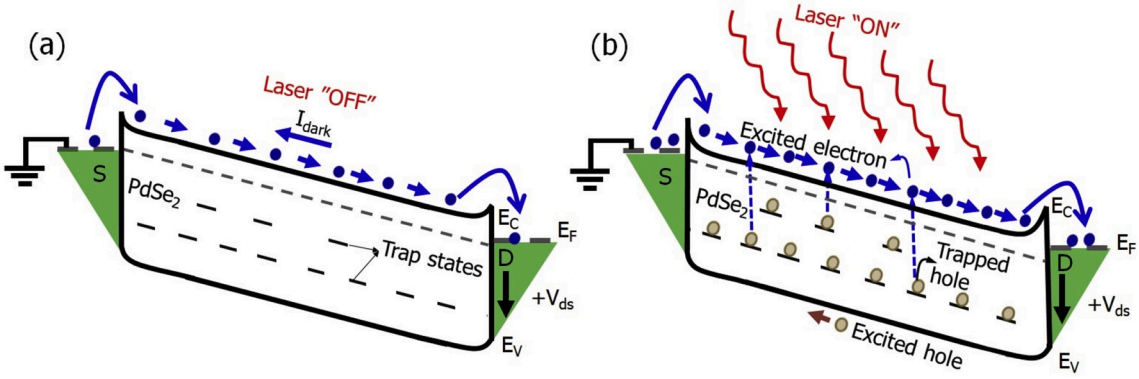

Fig. 5. Band diagram representations of $PdSe_2$-based photodetector device: (a) in the dark and (b) under laser illumination, that illustrate hole trapping in shallow and deeper trap states near the valence band.

$$I = I_o + A_1 exp\left(-t/_{t_1}\right) + A_1 exp\left(-t/_{t_2}\right). \quad (7)$$

We attributed the shorter decay component to the PC effect and shallower traps present in $PdSe_2$, and the longer decay component to the PG effect caused by the deeper (middle gap) traps, which are characterised by longer trapping/detrapping times [28,31,42]. In fact, these traps required longer exposure times to be filled, and yield the subsequent very long decay component.

4. Conclusion

In summary, we fabricated a few-layer $PdSe_2$ FET using a $PdSe_2$ nanobelt obtained using the conventional exfoliation technique. The photodetection capability of the as-fabricated $PdSe_2$ was tested at different P_{in} values. The $PdSe_2$ FET exhibited n-type characteristics, the on/off ratio of $\sim 10^4$, and a negative shift in V_t upon the increase in P_{in}. To understand the electrical transport at different P_{in} values, systematic data analyses were carried out. It was determined that charge trapping at the $PdSe_2/SiO_2$ interface and the defects in the $PdSe_2$ channel played significant roles in the observed conduction mechanism. Lastly, we demonstrated that the $PdSe_2$-based FET could be a suitable candidate for reproducible time-resolved photodetectors that require high photosensitivity. Our study could advance the research into $PdSe_2$-based FETs for photodetector applications.

Declaration of competing interest

The authors declare that they have no known competing financial interests or personal relationships that could have appeared to influence the work reported in this paper.

CRediT authorship contribution statement

A. Venkatesan: Conceptualization, Methodology, Formal analysis, Data curation, Visualization, Writing - original draft. **Servin Rathi:** Formal analysis, Validation, Writing - review & editing. **Yunseob Kim:** Software, Formal analysis. **Hanul Kim:** Software, Formal analysis. **Dongmok Whang:** Validation, Resources. **Sun Jin Yun:** Validation, Resources, Writing - review & editing. **Gil-Ho Kim:** Supervision, Validation, Resources, Writing - review & editing, Project administration, Funding acquisition.

Acknowledgement

This research was supported by Basic Science Research Program through the NRF funded by the Ministry of Education, Science and Technology (2018R1D1A1B07048985, 2019R1A2C2088719, and 2016R1D1A1B03932455) and Korea Research Fellowship Program through the NRF funded by the Ministry of Science and ICT (2015H1D3A1062519). This work was partly supported by the Institute for Information & Communications Technology Promotion grant funded by the Korea government (MSIT) (Grant No. 2016-0-00576, Fundamental technologies of two-dimensional materials and devices for the platform of new-functional smart devices).

References

[1] H. Fang, W. Hu, Photogating in low dimensional photodetectors, Adv. Sci. 4 (2017), 1700323.
[2] M. Long, P. Wang, H. Fang, W. Hu, Progress, challenges, and opportunities for 2D material based photodetectors, Adv. Funct. Mater. 29 (2019), 1803807.
[3] L. Wang, I. Meric, P.Y. Huang, Q. Gao, Y. Gao, H. Tran, T. Taniguchi, K. Watanabe, L.M. Campos, D.A. Muller, J. Guo, One-dimensional electrical contact to a two-dimensional material, Science 342 (2013) 614–617.
[4] K. Roy, M. Padmanabhan, S. Goswami, T.P. Sai, G. Ramalingam, S. Raghavan, A. Ghosh, Graphene–MoS_2 hybrid structures for multifunctional photoresponsive memory devices, Nat. Nanotechnol. 8 (2013) 826–830.
[5] M. Long, E. Liu, P. Wang, A. Gao, H. Xia, W. Luo, B. Wang, J. Zeng, Y. Fu, K. Xu, W. Zhou, Broadband photovoltaic detectors based on an atomically thin heterostructure, Nano Lett. 16 (2016) 2254–2259.
[6] D. Kufer, G. Konstantatos, Photo-FETs: phototransistors enabled by 2D and 0D nanomaterials, ACS Photonics 3 (2016) 2197–2210.
[7] G.H. Lee, Y.J. Yu, X. Cui, N. Petrone, C.H. Lee, M.S. Choi, D.Y. Lee, C. Lee, W. J. Yoo, K. Watanabe, T. Taniguchi, Flexible and transparent MoS_2 field-effect transistors on hexagonal boron nitride-graphene heterostructures, ACS Nano 7 (2013) 7931–7936.
[8] D.R. Chen, M. Hofmann, H.M. Yao, S.K. Chiu, S.H. Chen, Y.R. Luo, C.C. Hsu, Y. P. Hsieh, Lateral two-dimensional material heterojunction photodetectors with ultrahigh speed and detectivity, ACS Appl. Mater. Interfaces 11 (2019) 6384–6388.
[9] S.L. Li, L. Zhang, X. Zhong, M. Gobbi, S. Bertolazzi, W. Guo, B. Wu, Y. Liu, N. Xu, W. Niu, Y. Hao, Nano-subsidence assisted precise integration of patterned two-dimensional materials for high-performance photodetector arrays, ACS Nano 13 (2019) 2654–2662.
[10] J. Quereda, P. San-Jose, V. Parente, L. Vaquero-Garzon, A.J. Molina-Mendoza, N. Agraït, G. Rubio-Bollinger, F. Guinea, R. Roldán, Castellanos Gomez, A Strong modulation of optical properties in black phosphorus through strain-engineered rippling, Nano Lett. 16 (2016) 2931–2937.
[11] J. Choi, H. Zhang, J.H. Choi, Modulating optoelectronic properties of two-dimensional transition metal dichalcogenide semiconductors by photoinduced charge transfer, ACS Nano 10 (2016) 1671–1680.
[12] M. Long, A. Gao, P. Wang, H. Xia, C. Ott, C. Pan, Y. Fu, E. Liu, X. Chen, W. Lu, T. Nilges, Room temperature high-detectivity mid-infrared photodetectors based on black arsenic phosphorus, Sci. Adv. 3 (2017), 1700589.
[13] Z. Chen, X. Li, J. Wang, L. Tao, M. Long, S.J. Liang, L.K. Ang, C. Shu, H.K. Tsang, J. B. Xu, Synergistic effects of plasmonics and electron trapping in graphene short-wave infrared photodetectors with ultrahigh responsivity, ACS Nano 11 (2017) 430–437.
[14] D. Lloyd, X. Liu, J.W. Christopher, L. Cantley, A. Wadehra, B.L. Kim, B.B. Goldberg, A.K. Swan, J.S. Bunch, Band gap engineering with ultralarge biaxial strains in suspended monolayer, MoS_2 Nano Lett. 16 (2016) 5836–5841.
[15] L. Li, F. Yang, G.J. Ye, Z. Zhang, Z. Zhu, W. Lou, X. Zhou, L. Li, K. Watanabe, T. Taniguchi, K. Chang, Quantum Hall effect in black phosphorus two-dimensional electron system, Nat. Nanotechnol. 11 (2016) 593–597.
[16] Y. Jiao, F. Ma, J. Bell, A. Bilic, A. Du, Two-dimensional boron hydride sheets: high stability, massless Dirac fermions, and excellent mechanical properties, Angew. Chem. 128 (2016) 10448–10451.
[17] A. Nourbakhsh, A. Zubair, M.S. Dresselhaus, T. Palacios, Transport properties of a MoS_2/WSe_2 heterojunction transistor and its potential for application, Nano Lett. 16 (2016) 1359–1366.
[18] A. Avsar, I.J. Vera-Marun, J.Y. Tan, K. Watanabe, T. Taniguchi, A. Castro Neto, B. Ozyilmaz, Air-stable transport in graphene-contacted, fully encapsulated ultrathin black phosphorus-based field-effect transistors, ACS Nano 9 (2015) 4138–4145.
[19] A.D. Oyedele, S. Yang, L. Liang, A.A. Puretzky, K. Wang, J. Zhang, P. Yu, P. R. Pudasaini, A.W. Ghosh, Z. Liu, C.M. Rouleau, $PdSe_2$: pentagonal two-dimensional layers with high air stability for electronics, J. Am. Chem. Soc. 139 (2017) 14090–14097.
[20] G.D. Nguyen, L. Liang, Q. Zou, M. Fu, A.D. Oyedele, B.G. Sumpter, Z. Liu, Z. Gai, K. Xiao, A.P. Li, 3D imaging and manipulation of subsurface selenium vacancies in $PdSe_2$, Phys. Rev. Lett. 121 (2018), 086101.
[21] D. Qin, P. Yan, G. Ding, X. Ge, H. Song, G. Gao, Monolayer $PdSe_2$: a promising two-dimensional thermoelectric material, Sci. Rep. 8 (2018) 2764–2774.
[22] W.L. Chow, P. Yu, F. Liu, J. Hong, X. Wang, Q. Zeng, C.H. Hsu, C. Zhu, J. Zhou, X. Wang, J. Xia, High mobility 2D palladium diselenide field-effect transistors with tunable ambipolar characteristics, Adv. Mater. 29 (2017), 1602969.
[23] H. Zhong, Z. Zhang, H. Xu, C. Qiu, L.M. Peng, Comparison of mobility extraction methods based on field-effect measurements for graphene, AIP Adv. 5 (2015), 057136.
[24] D. Ovchinnikov, A. Allain, Y.S. Huang, D. Dumcencoand, A. Kis, Electrical transport properties of single-layer WS_2, ACS Nano 8 (2014) 8174–8181.
[25] W. Liu, J. Kang, D. Sarkar, Y. Khatami, D. Jena, K. Banerjee, Role of metal contacts in designing high-performance monolayer n-type WSe_2 field effect transistors, Nano Lett. 13 (2013) 1983–1990.
[26] F. Giubileo, A. Grillo, L. Iemmo, G. Luongo, F. Urban, M. Passacantando, A. Di Bartolomeo, Environmental effects on transport properties of $PdSe_2$ field effect transistors, Mater. Today: Proceedings 20 (2020) 50–53.
[27] Y.W. Tan, Y. Zhang, K. Bolotin, Y. Zhao, S. Adam, E.H. Hwang, S.D. Sarma, H. L. Stormer, P. Kim, Measurement of scattering rate and minimum conductivity in graphene, Phys. Rev. Lett. 99 (2007), 246803.
[28] M. Buscema, J.O. Island, D.J. Groenendijk, S.I. Blanter, G.A. Steele, H.S. van der Zant, A. Castellanos-Gomez, Photocurrent generation with two-dimensional van der Waals semiconductors, Chem. Soc. Rev. 44 (2015) 3691–3718.
[29] F. Xia, H. Wang, D. Xiao, M. Dubey, A. Ramasubramaniam, Two-dimensional material nanophotonics, Nat. Photon. 8 (2014) 899–907.
[30] H.S. Kang, C.S. Choi, W.Y. Choi, D.H. Kim, K.S. Seo, Characterization of phototransistor internal gain in metamorphic high-electron-mobility transistors, Appl. Phys. Lett. 84 (2004) 3780–3782.
[31] A. Di Bartolomeo, L. Genovese, T. Foller, F. Giubileo, G. Luongo, L. Croin, S. J. Liang, L.K. Ang, M. Schleberger, Electrical transport and persistent photoconductivity in monolayer MoS_2 phototransistors, Nanotechnology 28 (2017), 214002.
[32] S. Rathi, I. Lee, D. Lim, J. Wang, Y. Ochiai, N. Aoki, K. Watanabe, T. Taniguchi, G. H. Lee, Y.J. Yu, P. Kim, G.H. Kim, Tunable electrical and optical characteristics in

monolayer graphene and few-layer MoS_2 heterostructure devices, Nano Lett. 15 (2015) 5017–5024.
[33] J.W. Luginsland, Y.Y. Lau, R.M. Gilgenbach, Two-dimensional Child-Langmuir law, Phys. Rev. Lett. 77 (1996) 4668–4670.
[34] S. Ghatak, A. Ghosh, Observation of trap-assisted space charge limited conductivity in short channel MoS_2 transistor, Appl. Phys. Lett. 103 (2013), 122103.
[35] Y.S. Ang, M. Zubair, L.K. Ang, Relativistic space-charge-limited current for massive Dirac fermions, Phys. Rev. B 95 (2017), 165409.
[36] L.K. Ang, T.J. Kwan, Y.Y. Lau, New scaling of Child-Langmuir law in the quantum regime, Phys. Rev. Lett. 91 (2003), 208303.
[37] W. Choi, M.Y. Cho, A. Konar, J.H. Lee, G.B. Cha, S.C. Hong, S. Kim, J. Kim, D. Jena, J. Joo, S. Kim, High-detectivity multilayer MoS_2 phototransistors with spectral response from ultraviolet to infrared, Adv. Mater. 24 (2012) 5832–5836.
[38] M. Kang, S. Rathi, I. Lee, L. Li, M.A. Khan, D. Lim, Y. Lee, J. Park, S.J. Yun, D. H. Youn, C. Jun, G.H. Kim, Tunable electrical properties of multilayer $HfSe_2$ field effect transistors by oxygen plasma treatment, Nanoscale 9 (2017) 1645–1652.
[39] L. Zeng, L. Tao, C. Tang, B. Zhou, H. Long, Y. Chai, S.P. Lau, Y.H. Tsang, High-responsivity UV-vis photodetector based on transferable WS_2 film deposited by magnetron sputtering, Sci. Rep. 6 (2016), 20343.
[40] L.H. Zeng, D. Wu, S.H. Lin, C. Xie, H.Y. Yuan, W. Lu, S.P. Lau, Y. Chai, L.B. Luo, Z. J. Li, Y.H. Tsang, Controlled synthesis of 2D palladium diselenide for sensitive photodetector applications, Adv. Funct. Mater. 29 (2019), 1806878.
[41] Q. Liang, Q. Wang, Q. Zhang, J. Wei, S.X. Lim, R. Zhu, J. Hu, W. Wei, C. Lee, C. Sow, W. Zhang, High-performance, room temperature, ultra-broadband photodetectors based on air-stable $PdSe_2$, Adv. Mater. 31 (2019), 1807609.
[42] Y.C. Wu, C.H. Liu, S.Y. Chen, F.Y. Shih, P.H. Ho, C.W. Chen, C.T. Liang, W. H. Wang, Extrinsic origin of persistent photoconductivity in monolayer MoS_2 field effect transistors, Sci. Rep. 5 (2015), 11472.